PHOTONIC SENSORS / Vol. 8, No. 1, 2018: 70–79

Influence of Annealing on X-Ray Radiation Sensing Properties of TiO_2 Thin Film

M. P. SARMA[1], J. M. KALITA[1,2*], and G. WARY[1]

[1]*Department of Physics, Cotton University, Guwahati, 781001, India*

[2]*Department of Physics and Electronics, Rhodes University, P. O. Box 94, Grahamstown 6140, South Africa*

[*]Corresponding author: J. M. KALITA E-mail: jitukalita09@gmail.com

Abstract: A recent study shows that the titanium dioxide (TiO_2) thin film synthesised by a chemical bath deposition technique is a very useful material for the X-ray radiation sensor. In this work, we reported the influence of annealing on the X-ray radiation detection sensitivity of the TiO_2 film. The films were annealed at 333 K, 363 K, 393 K, 473 K, and 573 K for 1 hour. Structural analyses showed that the microstrain and dislocation density decreased whereas the average crystallite size increased with annealing. The band gap of the films also decreased from 3.26 eV to 3.10 eV after annealing. The *I-V* characteristics record under the dark condition and under the X-ray irradiation showed that the conductivity increased with annealing. The influence of annealing on the detection sensitivity was negligible if the bias voltage applied across the films was low (within 0.2 V – 1.0 V). At higher bias voltage (>1.0 V), the contribution of electrons excited by X-ray became less significant which affected the detection sensitivity.

Keywords: Titanium dioxide (TiO_2); thin film; annealing; X-ray; sensor

Citation: M. P. SARMA, J. M. KALITA, and G. WARY, "Influence of Annealing on X-Ray Radiation Sensing Properties of TiO_2 Thin Film," *Photonic Sensors*, 2018, 8(1): 70–79.

1. Introduction

Titanium dioxide (TiO_2) is a group IV-VI wide band gap semiconductor. Research concerning the optical and electrical properties of TiO_2 has been a subject of many researchers. TiO_2 exists in rutile, anatase, and brookite phase, and its band gap varies between 3.0 eV and 3.8 eV or even higher [1–4]. In general, the rutile phase is thermodynamically more stable than the anatase one [5], and the band gap of the anatase phase is higher than the rutile one [6].

TiO_2 has many unique optical and electrical properties which make it a favourable material for numerous applications, namely, photocatalysis [7], dye sensitised solar cells [8–10], gas sensors [11], pH sensor [12], light emitting diodes [1], and photodetectors [2, 13], etc. Apart from these applications, TiO_2 is also a very promising material for ultraviolet (UV) and X-ray sensors. Okuya *et al.* [3] reported that the TiO_2 film can be used as the UV detector, however, its detection sensitivity depends on the surface morphology and charge carrier density of the film. Fu and Cao [4] studied the UV sensitivity of the TiO_2 thin film and observed a large photogenerated current under UV light with the wavelength below 340 nm. Further, the results of Xing *et al.* [5] and Qi *et al.* [14] also supported that the TiO_2 thin film under UV radiation shows a high responsivity and a low dark current.

Received:10 October 2017 / Revised: 30 November 2017

DOI: 10.1007/s13320-017-0473-6
Article type: Regular

Regarding X-ray sensitivity, Sarma *et al.* [15], for the first time, showed that the TiO_2 thin film synthesised by a chemical bath deposition (CBD) technique could be used to detect X-ray radiation. There are many advantages of the TiO_2 thin film to be used as an X-ray sensor. For example, it can be synthesised by the CBD technique. CBD is the cheapest technique to synthesise the thin film, and therefore it enables one to design a cost-effective X-ray sensor. Moreover, TiO_2 is more stable in the common environment than other chalcogenides. Therefore, the longevity of the sensor would be high.

Although the TiO_2 films show a great potential for the X-ray sensor, the sensitivity of the film may be affected by annealing temperature, because the physical properties of many thin films often change due to post-annealing treatment. Naceur *et al.* [6] studied the effect of annealing on optical properties of nanostructured TiO_2 thin films. The shape and density of the nanocrystalline structure of the films were found to depend on the annealing temperature. It was reported that the crystalline phase of the films changed from anatase to rutile after annealing at 1273 K [6]. Lin *et al.* [16] observed that the crystallite size increased whereas the band gap decreased with annealing temperature. Further, the photocatalytic activity of the films was found to be improved with annealing at 673 K [16]. Zulkefle *et al.* [17] reported that the roughness of the film increased with annealing. The annealing temperature was also found to affect the sensitivity of extended-gate field effect transistor based portable pH sensor [18]. The pH sensitivity of the sensor decreased with annealing temperature [18].

As cited earlier, Sarma *et al.* [15] recently showed the potential application of the TiO_2 film as the X-ray radiation sensor. For a material to be used as a radiation detector, it will be advantageous from the practical point of view if the material can sustain high temperature. Literature showed that many physical characteristics, for example, crystallite size, phase, roughness, and band gap of the TiO_2 thin film were affected by annealing temperature. Therefore, it is important to study the X-ray radiation sensitivity of the film annealed at different temperatures. In this work, we reported on the influence of annealing on the X-ray detection sensitivity of the film.

2. Experimental details

There are several methods for thin film deposition. Among them, we used a chemical bath deposition method to prepare the TiO_2 thin films. For synthesis, we followed the same protocol as reported in our previous work [15]. In the previous study, it was noted that the films prepared at 3.0 M had superior electrical conductivity than the relatively lower molarity films, and the 3.0 M film was more sensitive for X-ray detection [15]. Therefore, in this study, the annealing treatment was carried out on the films prepared at 3.0 M. To prepare the 3.0 M films, titanium (IV) iso-propoxide of 3.0 M was added with propanol of the same molarity and stirred continuously. The solution bath temperature was maintained at 353 K. The pH of the solution was monitored and maintained between 2.0 and 2.3 by adding glacial acetic acid. After 1 hour of stirring, chemically cleaned glass substrates were immersed in the solution beaker. The glass substrates covered with TiO_2 layers were taken out after 24 hours and dried in air. The details of the deposition technique were discussed in our previous report [15]. The presence of essential elements, i.e. the Ti and O, was confirmed by an X-ray fluorescence spectroscopic analysis [15]. To study the annealing effect, the films were annealed in air at 333 K, 363 K, 393 K, 473 K, and 573 K for 1 hour by an electronic temperature controlled muffle furnace.

To study the influence of annealing on the structural parameters of the films, X-ray diffraction (XRD) patterns were recorded by an X-ray diffractometer (Rigaku-TTRAX III, Japan, λ = 1.5406 Å for Cu Kα radiation, V = 50 kV, and I =

180 mA). On the other hand, to examine any influence of annealing on the surface morphology of the films, a surface morphological analysis was carried out using a field-emission scanning electron microscope (FE-SEM) (ZEISS SIGMA VP, Germany).

To study the effect of annealing on the optical properties of the films, the optical absorption spectrum was recorded within 250 nm to 800 nm using a UV-vis spectrometer (CARY-300, Varian, Australia). Further, the current-voltage (*I-V*) characteristics of the films were recorded by a digital electrometer (Keithley, 6517B, United States). Aluminium was used as a connecting electrode, and the potential was applied by a variable direct current (DC) power supply. For X-ray radiation, unless otherwise stated, the X-ray tube was operated at 35 kV source potential and 15 mA filament current. The source emited X-ray of wavelength 1.5406 Å.

3. Results and discussions

3.1 Structural and surface morphological analyses

Figure 1 shows the XRD patterns of the films annealed at 333 K, 363 K, 393 K, 473 K, and 573 K. For comparison, the XRD pattern of the un-annealed film is also shown. The diffraction patterns were recorded within 20° to 70° at a resolution of 0.03° in 2θ scale. The peaks are indexed according to the Joint Committee on Powder Diffraction Standard (JCPDS) data file 21-1272. The patterns indicate the anatase phase of TiO_2. It seems from Fig. 1 that the diffraction peaks are stable with annealing up to 573 K. This implies that the crystalline nature of the films did not change after annealing up to 573 K.

The XRD peaks of the annealed films are analysed to study any structural change caused by annealing. Some structural parameters such as crystallite size, microstrain, and dislocation density are evaluated. Using Scherrer's equation [19], the average crystallite size corresponding to the films annealed at 333 K, 363 K, 393 K, 473 K, and 573 K is estimated as 6.6 nm, 6.9 nm, 7.3 nm, 8.1 nm, and 8.3 nm, respectively. Scherrer's equation estimates the crystallite size using the broadening of a diffraction peak where the influence of non-uniform internal strain (so called microstrain) towards broadening of the peak is neglected. It is known that the broadening of XRD peaks occurs due to the simultaneous contribution of both crystallite size and internal strain. Therefore, the crystallite size calculated using Scherrer's equation slightly differs from the actual size. In order to calculate the reliable value of the crystallite size and the possible microstrain, the Williamson-Hall (W-H) analysis [20] is carried out. According to the theory of W-H, the full width at half maxima β of a multiple ordered diffraction peak can be expressed as

$$\beta = (\lambda / D\cos\theta) + 4\varepsilon\tan\theta \quad (1)$$

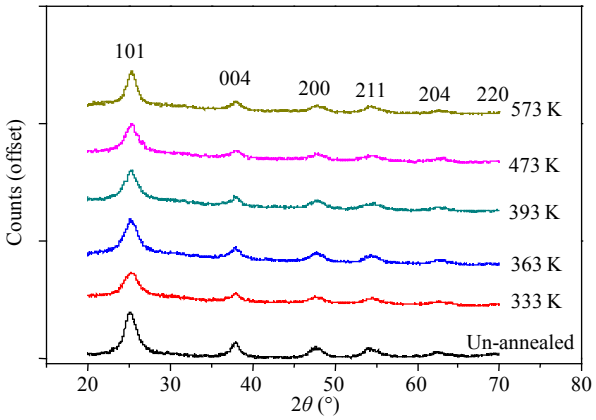

Fig. 1 XRD patterns of an un-annealed and 333 K, 363 K, 393 K, 473 K, and 573 K annealed films.

where λ is the wavelength of X-ray, θ is the diffraction angle, ε is the microstrain presenting in the crystal lattice, and D is the average crystallite size. Equation (1) implies that a plot of $(\beta\cos\theta)/\lambda$ against $(2\sin\theta)/\lambda$ is linear with the slope 2ε and intercept equal to $1/D$. Using the plot, the average crystallite sizes of the films annealed at 333 K, 363 K, 393 K, 473 K, and 573 K are calculated as 8.7 nm, 8.8 nm, 9.2 nm, 10.1 nm, and 10.2 nm, respectively. Further, the microstrains presenting in the corresponding films are calculated as 3.83×10^{-3},

3.47×10^{-3}, 3.34×10^{-3}, 2.89×10^{-3}, and 2.78×10^{-3}. For the un-annealed film, the average crystallite size was found as 8.6 nm and the microstrain as 5.01×10^{-3} [15]. The slight difference in the crystallite size estimated using Scherrer's equation and W-H analysis is due to the influence of strain in the crystal lattice. The minimum dislocation density which is numerically equal to $1/D^2$ is calculated from the average crystallite size [21]. For the films annealed at 333 K, 363 K, 393 K, 473 K, and 573 K, the minimum dislocation density is calculated as 2.29×10^{16}, 2.10×10^{16}, 1.88×10^{16}, 1.52×10^{16}, and 1.45×10^{16} lines/m^2, respectively. In comparison, the minimum dislocation density for the un-annealed film is calculated as 2.52×10^{16} lines/m^2 [15].

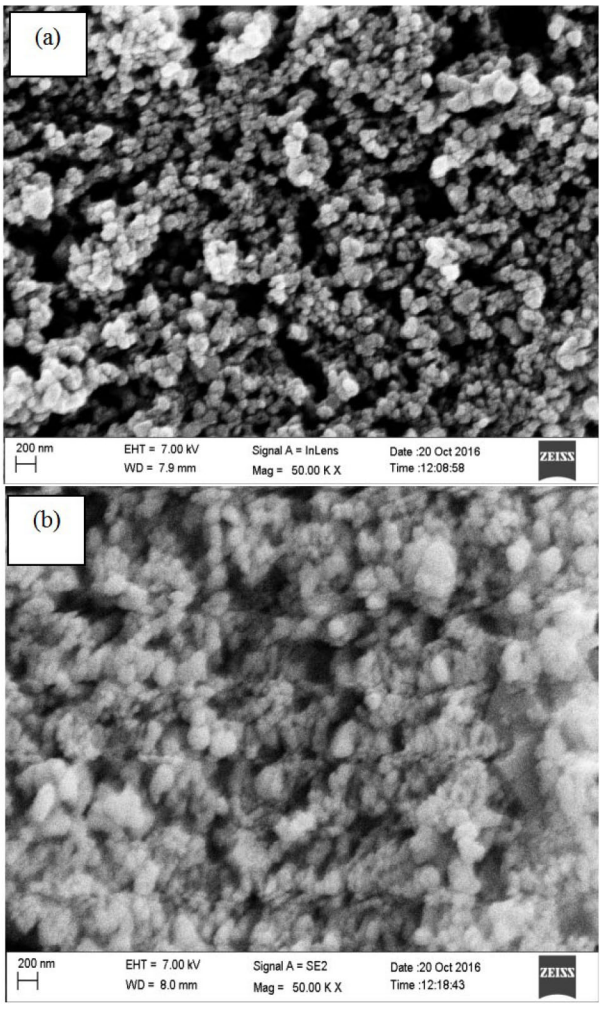

Fig. 2 Field-emission scanning electron microscopic images of (a) 393 K-annealed and (b) un-annealed films under 50 K magnification.

The microstrain and minimum dislocation density are found to decrease, and the average crystallite size is found to increase with annealing. Lin *et al.* [16] also found a similar increase in the crystallite size with annealing. An increase in the crystallite size and a decrease in the microstrain as well as the dislocation density are due to the thermally induced coalescence of smaller grains at the grain boundary. At higher annealing temperatures, the atoms in the films have adequate diffusion activation energy to reside in the thermodynamically favourable sites within the crystal lattice, and in due course the smaller grains having lower surface energy become larger [22, 23].

In order to study any influence of annealing on the surface morphology of the films, FE-SEM analysis is carried out. Figure 2 shows FE-SEM micrographs of an un-annealed and the 393 K annealed films under the same magnification. The surfaces of the films are homogeneous and constituted by some smaller as well as relatively larger agglomerated grains. Due to annealing, a little change in the grain structures is found (see Fig. 2).

3.2 Optical properties

To study the effect of annealing on the absorption edge, the absorption spectra of the films were recorded. Figure 3(a) shows the absorption spectra recorded from the films annealed at 333 K, 363 K, 393 K, 473 K, and 573 K. For all the films, an absorption peak was observed within 300 nm to 320 nm, and the absorbance of the films seemed to be increased with annealing. The band gap of the annealed films was estimated from Tauc's equation [24]. Figure 3(b) shows Tauc's plots corresponding to the absorption spectra recorded from the films annealed at 333 K, 363 K, 393 K, 473 K, and 573 K. This analysis gives the band gap of the 333 K, 363 K, 393 K, 473 K, and 573 K annealed films as 3.21 eV, 3.16 eV, 3.14 eV, 3.13 eV, and 3.10 eV, respectively. In contrast, the band gap of an un-annealed film was 3.26 eV [15]. The band gap of the films is found to

decrease with annealing. A decrease in the band gap of the annealed films can be attributed to some structural changes occurring during annealing [25]. It is evident from preceding structural analyses that the crystallite size increased with annealing temperature whereas microstrain in the lattice decreased with annealing. Due to these changes, the dislocation density in the films decreased with annealing temperature. A decrease in the dislocation density in the crystal lattice reduces the defect induced energy states, which in turn decreases the band gap of the film.

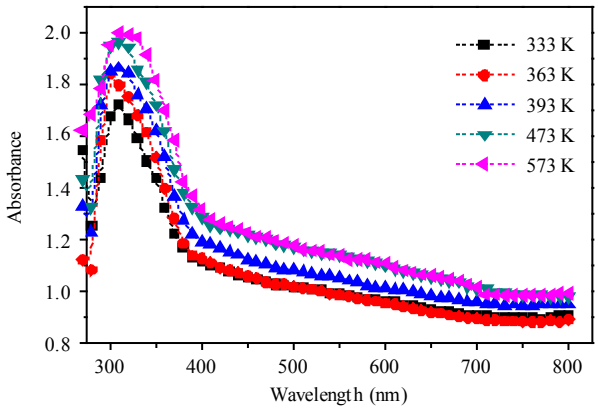

Fig. 3 Absorption spectra recorded from the TiO_2 films annealed at 333 K, 363 K, 393 K, 473 K, and 573 K (the dotted lines are visual guides) (a) and Tauc's plots to the absorption spectra of the 333 K, 363 K, 393 K, 473 K, and 573 K annealed films (b).

3.3 Current-voltage (*I-V*) characteristics

To measure the *I-V* characteristic, aluminium was used as an electrode. The work function of aluminium is 4.170 eV [26] whereas that of the TiO_2 is 4.899 eV [27]. Owing to the lower work function of aluminium than that of the TiO_2, the contact between the electrode and the film was ohmic. As a result, the current through an un-annealed film was found to increase uniformly with the bias voltage [15]. In the present case, the *I-V* characteristics of the annealed films were first recorded under the dark condition and later under the X-ray irradiation using the same experimental setup as discussed by Sarma *et al.* [28]. Figure 4 shows the *I-V* characteristics recorded from the films annealed at 333 K, 363 K, 393 K, 473 K, and 573 K. The same characteristics corresponding to the un-annealed film reported by Sarma *et al.* [15] were also shown for ease of comparison. The results shown in Fig. 4 are the average of three identical measurements, and the corresponding error bars represent their standard deviations. In all the cases, the *I-V* characteristics were found to follow Ohm's law, and the current under X-ray irradiation was significantly higher than that under the dark condition. Under the dark condition, the initial start-up currents of the annealed films were found to flow at relatively lower bias voltage than that in the un-annealed film [see Fig. 4(a)]. This is due to a decrease in the band gap with annealing.

The electrical conductivity of the films was calculated from the *I-V* characteristics. For the films annealed at 333 K, 363 K, 393 K, 473 K, and 573 K, the conductivities under the dark condition were calculated as 1.81×10^{-2} S/cm, 2.14×10^{-2} S/cm, 6.60×10^{-2} S/cm, 1.29×10^{-1} S/cm, and 1.75×10^{-1} S/cm whereas those under the X-ray irradiation were 2.96×10^{-1} S/cm, 3.53×10^{-1} S/cm, 6.77×10^{-1} S/cm, 1.75 S/cm, and 2.03 S/cm, respectively. In comparison, the conductivity of the un-annealed film under the dark condition was found as 1.11×10^{-2} S/cm whereas that under the X-ray irradiation was 2.22×10^{-1} S/cm [15]. For all the films, the conductivity under the X-ray irradiation was found to be greater than that under the dark condition. This was in accordance with the model

which was used to discuss the conductivity of the ZnS thin film [28] as well as that for the un-annealed TiO_2 film [15]. According to the model, the current under the dark condition is only due to the electrons excited by the bias voltage whereas the current under the X-ray irradiation is contributed by the electrons simultaneously excited due to the applied bias voltage and the high energy radiation (i.e., X-ray). Under the X-ray irradiation, the excess electrons generated by the X-ray contribute more current and therefore show greater conductivity than that under the dark condition [15, 28].

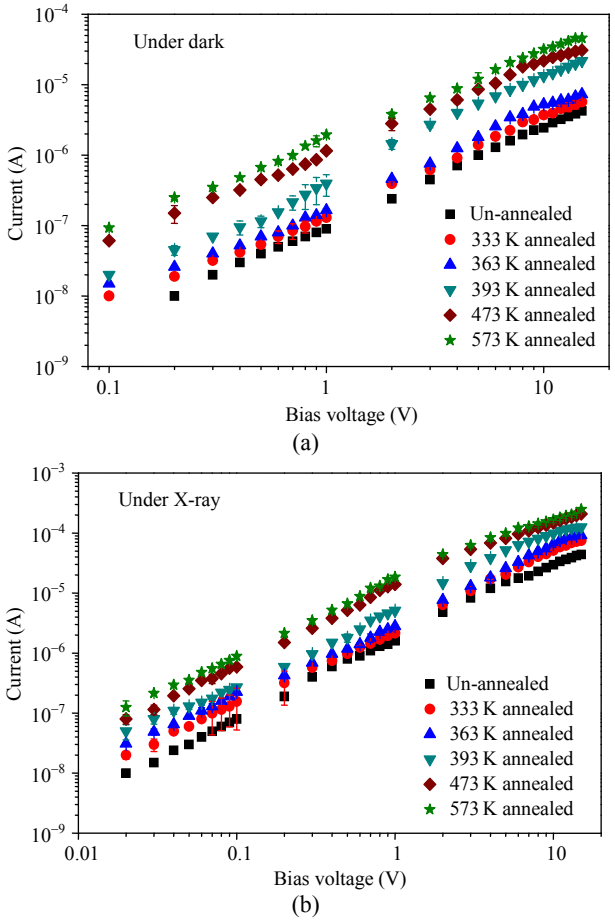

Fig. 4 *I-V* characteristics of an un-annealed and 333 K, 363 K, 393 K, 473 K, and 573 K annealed films recorded under the (a) dark condition and (b) X-ray radiation condition.

Regarding the influence of annealing, the conductivity under the dark condition as well as that under the X-ray irradiation was found to increase with annealing. An increase in conductivity could be ascribed to a decrease in the grain boundary as well as the band gap of the material. A similar increase in conductivity with annealing was also observed in the ZnS film [29].

3.4 X-ray detection sensitivity

The detection sensitivity S for a particular energy of X-ray irradiation was calculated as a function of the bias voltage (V) using the relation $S(V) = (I_r - I_d) / I_d$. Here, I_r is the current at a bias voltage V measured during the X-ray irradiation (the X-ray is generated by the source at 35 kV and 15 mA filament current), and I_d is the dark current at the corresponding bias voltage. Figure 5 shows a plot of detection sensitivity of the annealed films against the bias voltages (V). The same feature of the un-annealed film is also shown for reference. The detection sensitivity of the films after annealing was found to be affected to some extent. The sensitivity of the un-annealed film was constant within 0.2 V – 2.0 V [15]. On the other hand, the sensitivity of the films annealed at 333 K and 363 K was constant within 0.2 V – 4.0 V. Further, the sensitivity of the films annealed at 393 K, 473 K, and 573 K was constant within 0.2 V – 2.0 V and decreased thereafter. Moreover, some fluctuation in the sensitivity was found as the annealing temperature increased. The differences in the variation of sensitivity with annealing were mostly due to the change of the band gap as well as some structural and surface morphological changes.

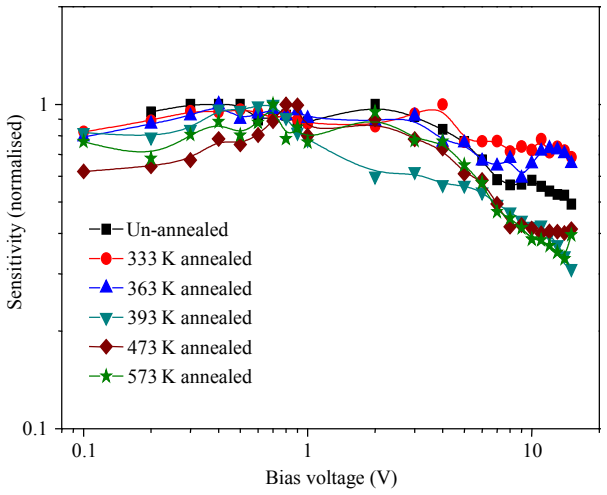

Fig. 5 Detection sensitivity of an un-annealed and 333 K, 363 K, 393 K, 473 K, and 573 K annealed films against the bias voltage.

The preceding analysis shows that the detection sensitivity of all the films corresponding to X-ray generated by the source at 35 kV source potential and 15 mA filament current is constant mostly between 0.2 V and 2.0 V bias voltage. In order to study the sensitivity for different energies of the X-ray radiation, the current flowing through the films for the bias voltages between 0.2 V and 2.0 V was studied by changing the energy of the X-ray radiation. In this experiment, the energy of the X-ray was varied by changing the X-ray source potential between 25 kV and 35 kV while keeping the filament current constant at 15 mA. Figure 6 shows the current passing through the un-annealed and annealed films for bias voltages $V = 0.7$ V, 0.9 V, 1.0 V, and 2.0 V. Each data point is the mean of three identical measurements, and the error bars are their corresponding standard deviations. The current in all the films was found to increase with the X-ray source potential. For quantitative analysis, the slope of the curves was calculated for all bias voltages. The magnitude of the slopes corresponding to the un-annealed and 333 K, 363 K, 393 K, 473 K, and 573 K annealed films for bias voltage, $V = 0.7$ V, 0.9 V, 1.0 V, and 2.0 V are reported in Table 1. It is evident in Table 1 that the magnitudes of the slopes are consistent for all the annealed and un-annealed films. However, for higher bias voltage, for example, $V = 2.0$ V, some deviation of the slopes was observed among the annealed films. The consistency in the slopes implies that a rate of increase in the current per unit change of X-ray energy is the same for the un-annealed and annealed films provided the bias voltage is low (within 0.2 V – 1.0 V). At higher bias voltage (>1.0 V), owing to the lower band gap of relatively higher temperature annealed films, the number of electrons excited to the conduction band by X-ray becomes less significant than those excited by the applied bias voltage. As a result, the sensitivity of the film changes.

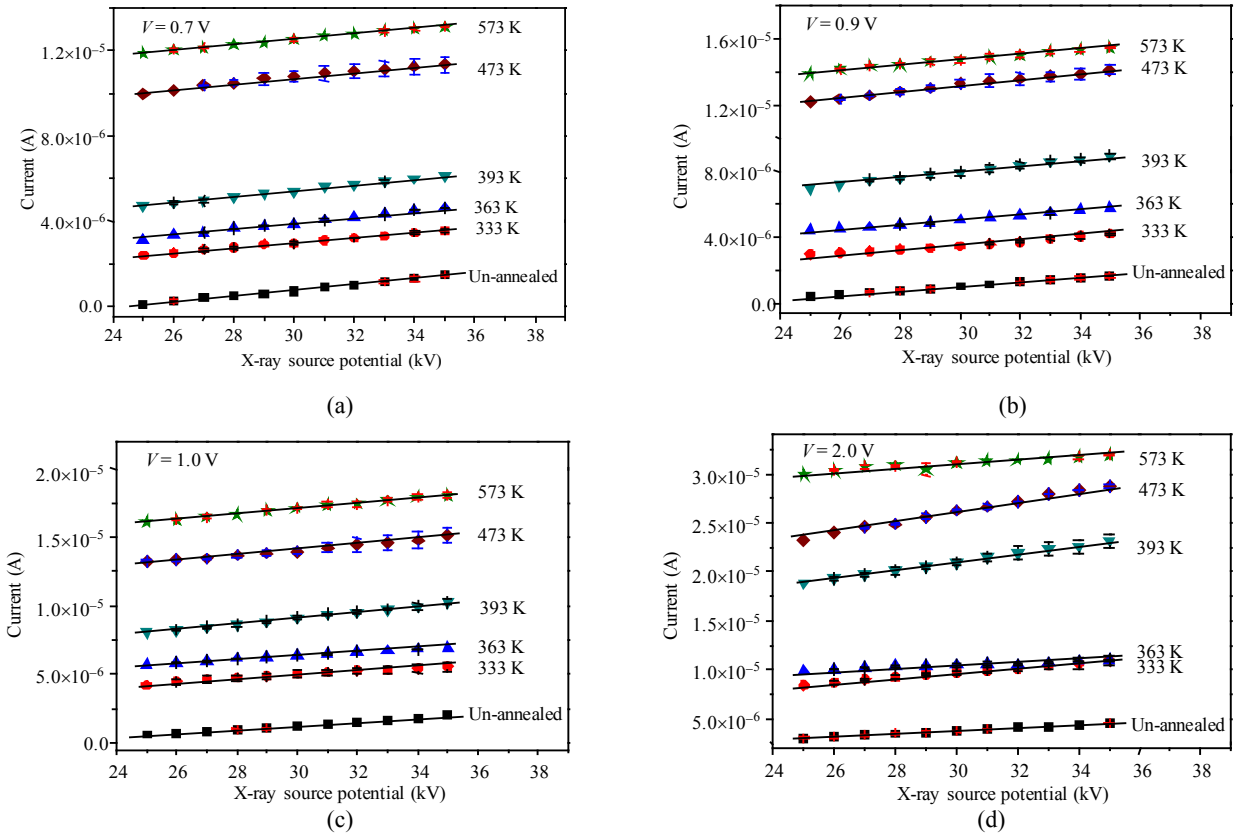

Fig. 6 Variation of current with X-ray source potential for the un-annealed and 333 K, 363 K, 393 K, 473 K, and 573 K annealed films corresponding to bias voltage: (a) $V = 0.7$ V, (b) $V = 0.9$ V, (c) $V = 1.0$ V, and (d) $V = 2.0$ V.

Table 1 Slope of the plots shown in Fig. 6.

Sample	Bias voltage (V)	$\|Slope\|\times10^{-7}$
Un-annealed	0.7	1.32±0.02
333 K annealed		1.14±0.02
363 K annealed		1.47±0.03
393 K annealed		1.43±0.02
473 K annealed		1.37±0.06
573 K annealed		1.27±0.02
Un-annealed	0.9	1.22±0.02
333 K annealed		1.24±0.05
363 K annealed		1.38±0.04
393 K annealed		1.89±0.04
473 K annealed		1.90±0.05
573 K annealed		1.48±0.04
Un-annealed	1.0	1.39±0.04
333 K annealed		1.26±0.05
363 K annealed		1.23±0.03
393 K annealed		1.16±0.04
473 K annealed		1.87±0.07
573 K annealed		1.99±0.04
Un-annealed	2.0	1.50±0.02
333 K annealed		2.48±0.05
363 K annealed		1.01±0.06
393 K annealed		4.25±0.07
473 K annealed		5.52±0.12
573 K annealed		1.75±0.17

3.5 Stability of the films

In the common environment, the quality of some thin films degrades with time due to moisture and dust particles presenting in the atmosphere. For practical applications of a film, it is necessary to study any potential degradation of the quality of the films in the common environment. To study such effects, the films were kept in an open place inside a room, and *I-V* characteristics of the films were recorded under the dark condition as well as under the X-ray irradiation condition. The experiment was repeated up to 15 days from the 1st day of synthesis of the film. It was observed that the *I-V* characteristics of the films measured between the 1st day and 15th day were approximately the same. Figure 7 shows the variation of conductivity of the un-annealed film against the time between the day of synthesis and measurement of the *I-V* characteristics. It is evident that the conductivity of the film under both dark and X-ray irradiation conditions are consistent with time. The statistical coefficient of variation in the conductivity of the un-annealed film was about 1.37% under the dark condition and was about 1.72% under the X-ray irradiation condition. The similar consistency in conductivity was also found in the annealed films. However, for visual clarity, the relevant plots are not shown in Fig. 7. Therefore, from this analysis, it can be concluded that the films are stable in the common environment.

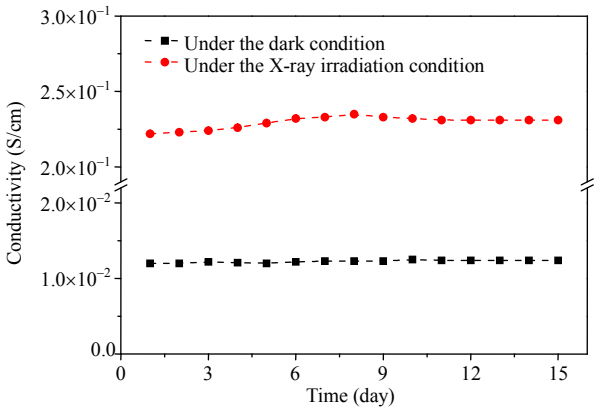

Fig. 7 Variation of conductivity of the un-annealed film against time.

4. Conclusions

The effect of annealing on the X-ray radiation detection sensitivity of the TiO_2 thin film synthesised by a chemical bath deposition technique has been studied. The films were annealed at 333 K, 363 K, 393 K, 473 K, and 573 K for 1 hour. The structural analysis showed that the crystalline nature of the films did not change after annealing up to 573 K. However, the microstrain and minimum dislocation density were found to decrease, and the average crystallite size was found to increase with annealing. Further, the analysis of the absorption spectra showed that the band gap of the films decreased with annealing. The *I-V* characteristics of the films were studied under the dark condition and under the X-ray irradiation. Under both conditions,

the conductivities were found to increase with annealing temperature. The increase in conductivity was attributed to the decrease in the band gap as well as the structural changes occurred during annealing. Regarding the detection sensitivity of X-ray, the influence of annealing was negligible if the bias voltage applied across the films was low. The higher bias voltage lessened the contribution of electrons excited by the X-ray which affected the detection sensitivity of the annealed films.

Acknowledgment

Authors thank the Department of Physics, Indian Institute of Technology (IIT), Guwahati for providing the XRD facility; Department of Physics, Gauhati University for the UV-Vis absorption spectra; Institute of Advanced Studies in Science and Technology (IASST), Guwahati for the FESEM report.

References

[1] Y. Liu, C. R. Gorla, S. Liang, N. Emanetoglu, Y. Lu, H. Shen, *et al.*, "Ultraviolet detectors based on epitaxial ZnO films grown by MOCVD," *Journal of Electronic Materials*, 2000, 29(1): 69–74.

[2] Y. Saito, S. Kambe, T. Kitamura, Y. Wada, and S. Yanagida, "Morphology control of mesoporous TiO_2 nanocrystalline films for performance of dye-sensitized solar cells," *Solar Energy Materials & Solar Cells*, 2004, 83(1): 1–13.

[3] M. Okuya, K. Shiozaki, N. Horikawa, T. Kosugi, G. R. A. Kumara, J. Madarasz, *et al.*, "Porous TiO_2 thin films prepared by spray pyrolysis deposition (SPD) technique and their application to UV sensors," *Solid State Ionics*, 2004, 172(1–4): 527–531.

[4] Y. Fu and W. H. Cao, "Preparation of transparent TiO_2 nanocrystalline film for UV sensor," *Chinese Science Bulletin*, 2006, 51(14): 1657–1661.

[5] J. Xing, H. Y. Wei, E. J. Guo, and F. Yang, "Highly sensitive fast-response UV photodetectors based on epitaxial TiO_2 films," *Journal of Physics D: Applied Physics*, 2011, 44(37): 375104-1 –375104-5.

[6] J. B. Naceur, M. Gaidi, F. Bousbih, R. Mechiakh, and R. Chtourou, "Annealing effects on microstructural and optical properties of nanostructured-TiO_2 thin films prepared by sole gel technique," *Current Applied Physics*, 2012, 12: 422–428.

[7] M. Schiavello, *Heterogeneous photocatalysis*, *Wiley Series in Photoscience and Photoengineering*. Chichester, England: John Wiley & Sons, 1997: 1–208.

[8] S. Duenas, H. Castan, H. Garcia, E. S. Andres, M. T. Luque, I. Martil, *et al.*, "A comparative study of the electrical properties of TiO_2 films grown by high-pressure reactive sputtering and atomic layer deposition," *Semiconductor Science & Technology*, 2005, 20(10): 1044–1051.

[9] R. S. Mane, Y. H. Hwang, C. D. Lokhande, S. D. Sartale, and S. H. Han, "Room temperature synthesis of compact TiO_2 thin films for 3-D solar cells by chemical arrested route," *Applied Surface Science*, 2005, 246(1–3): 271–278.

[10] S. J. Darzi, A. R. Mahjoub, and A. Nilchi, "Investigation of structural, optical and photocatalytic properties of mesoporous TiO_2 thin film synthesized by sol-gel templating technique," *Physica E: Low-dimensional Systems and Nanostructures*, 2009, 42(2): 176–181.

[11] Y. Shimizu and M. Egashira, "Basic aspects and challenges of semiconductor gas sensors," *MRS Bulletin*, 1999, 24(6): 18–24.

[12] Y. Matsumtao, M. Murakami, T. Shona, T. Hasegawa, T. Fukumura, M. Kawasaki, *et al.*, "Room-temperature ferromagnetism in transparent transition metal-doped titanium dioxide," *Science*, 2001, 291(5505): 854–856.

[13] A. N. Kulkarni, M. B. R. Prasad, H. M. Pathan, and R. S. Patil, "TiO_2 photoanode sensitized with nanocrystalline Bi_2S_3: the effect of sensitization time and annealing on its photovoltaic performance," *Applied Nanoscience*, 2016, 6(4): 567–574.

[14] H. F. Qi, D. B. Liu, and F. L. Sun, "The fabrication and characterization of TiO_2 UV detector," in *Proceeding of 28th Int. Congress of the Aeronautical Sciences*, Brisbane, Australia, 2012, pp. 60–69.

[15] M. P. Sarma, J. M. Kalita, and G. Wary, "Chemical bath deposited nanocrystalline TiO_2 thin film as X-ray radiation sensor," *Materials Research Express*, 2017, 4(4): 045005-1–045005-10.

[16] C. P. Lin, H. Chen, A. Nakaruk, P. Koshy, and C. C. Sorrell, "Effect of annealing temperature on the

photocatalytic activity of TiO_2 thin films energy," *Energy Procedia*, 2103, 34: 627–636.

[17] M. A. Zulkefle, R. A. Rahman, K. A. Yusoff, W. F. H. Abdullah, M. Rusop, and S. H. Herman, "Post-deposition annealing temperature dependence TiO_2-based EGFET pH sensor sensitivity," in *Proceeding of International Conference on Nano-Electronic Technology Devices and Materials*, Selangor, Malaysia, 2015, pp. 1–20.

[18] P. C. Yao, M. C. Lee, and J. L. Chiang, "Annealing effect of sol-gel TiO_2 thin film on pH-EGFET sensor," in *Proceeding of International Symposium on Computer, Consumer and Control (IS3C)*, Taiwan, China, 2014, pp. 577–580.

[19] B. D. Cullity, *Elements of X-ray diffraction*. London, England: Addison-Wesley Publishing Co., Inc, 1978: 1–664.

[20] G. K. Williamson and W. H. Hall, "X-ray line broadening from filed aluminium and wolfram," *Acta Metallurgica*, 1953, 1(1): 22–31.

[21] G. K. Williamson and R. E. Smallman, "Dislocation densities in some annealed and cold-worked metals from measurements on the X-ray debye-scherrer spectrum," *Philosophical Magazine Series 1*, 1956, 1(1): 34–46.

[22] Y. Caglar, S. Ilican, M. Caglar, F. Yakuphanoglu, J. Wu, and K. Gao, "Influence of heat treatment on the nanocrystalline structure of ZnO film deposited on p-Si," *Journal of Alloys & Compounds*, 2009, 481(1): 885–889.

[23] J. Sengupta, R. K. Sahoo, K. K. Bardhan, and C. D. Mukheijee, "Influence of annealing temperature on the structural, topographical and optical properties of sol-gel derived ZnO thin films," *Materials Letters*, 2011, 65(17): 2572–2574.

[24] J. Tauc, R. Grigorovici, and A. Vancu, "Optical properties and electronic structure of amorphous Ge and Si," *Materials Research Bulletin*, 1968, 3(1): 37–46.

[25] H. Ahn and Y. Um, "Post-annealing effects on ZnS thin films grown by using the CBD method," *Journal of the Korean Physical Society*, 2015, 67(6): 1045–1050.

[26] J. I. Pankove, *Optical processes in semiconductors*. New York, USA: Dover Publications, 1971: 36–94.

[27] G. X. R. Smith, R. Crook, and J. D Wadhawan, "Measuring the work function of TiO_2 nanotubes using illuminated electrostatic force microscopy," *Journal of Physics: Conference Series*, 2013, 471: 012045-1–012045-4.

[28] M. P. Sarma, J. M. Kalita, and G. Wary, "Chemically deposited ZnS thin film as potential X-ray radiation sensor," *Materials Science in Semiconductor Processing*, 2017, 61: 131–136.

[29] M. P. Sarma, J. M. Kalita, and G. Wary, "X-ray radiation sensing properties of ZnS thin film: a study on the effect of annealing," *Chinese Physics Letters*, 2017, 34(7): 262–265.